



# Human platelet lysate biotherapy for traumatic brain injury: preclinical assessment

Ouada Nebie,<sup>1,2,3</sup> Kevin Carvalho,<sup>2,3</sup> Lassina Barro,<sup>4</sup> Liling Delila,<sup>1</sup> Emilie Faivre,<sup>2,3</sup> Ting-Yi Renn,<sup>5</sup> Ming-Li Chou,<sup>1,6,†</sup> Yu-Wen Wu,<sup>1</sup> Ariunjargal Nyam-Erdene,<sup>4</sup> Szu-Yi Chou,<sup>7,8,9</sup> Luc Buée,<sup>2,3,10</sup> Chaur-Jong Hu,<sup>7,8,9,11,12</sup> Chih-Wei Peng,<sup>4,13</sup> David Devos,<sup>2,10</sup> David Blum<sup>2,3,9,‡</sup> and  Thierry Burnouf<sup>1,4,6,13,14,15,‡</sup>

‡These authors contributed equally to this work.

Traumatic brain injury (TBI) leads to major brain anatomopathological damages underlined by neuroinflammation, oxidative stress and progressive neurodegeneration, ultimately leading to motor and cognitive deterioration. The multiple pathological events resulting from TBI can be addressed not by a single therapeutic approach, but rather by a synergistic biotherapy capable of activating a complementary set of signalling pathways and providing synergistic neuroprotective, anti-inflammatory, antioxidative, and neurorestorative activities. Human platelet lysate might fulfil these requirements as it is composed of a plethora of biomolecules readily accessible as a TBI biotherapy.

In the present study, we tested the therapeutic potential of human platelet lysate using *in vitro* and *in vivo* models of TBI. We first prepared and characterized platelet lysate from clinical-grade human platelet concentrates. Platelets were pelletized, lysed by three freeze-thaw cycles, and centrifuged. The supernatant was purified by 56°C 30 min heat treatment and spun to obtain the heat-treated platelet pellet lysate that was characterized by ELISA and proteomic analyses. Two mouse models were used to investigate platelet lysate neuroprotective potential. The injury was induced by an in-house manual controlled scratching of the animals' cortex or by controlled cortical impact injury. The platelet lysate treatment was performed by topical application of 60 µl in the lesioned area, followed by daily 60 µl intranasal administration from Day 1 to 6 post-injury.

Platelet lysate proteomics identified over 1000 proteins including growth factors, neurotrophins, and antioxidants. ELISA detected several neurotrophic and angiogenic factors at ~1–50 ng/ml levels. We demonstrate, using two mouse models of TBI, that topical application and intranasal platelet lysate consistently improved mouse motor function in the beam and rotarod tests, mitigated cortical neuroinflammation, and oxidative stress in the injury area, as revealed by downregulation of pro-inflammatory genes and the reduction in reactive oxygen species levels. Moreover, platelet lysate treatment reduced the loss of cortical synaptic proteins. Unbiased proteomic analyses revealed that heat-treated platelet pellet lysate reversed several pathways promoted by both controlled cortical impact and cortical brain scratch and related to transport, postsynaptic density, mitochondria or lipid metabolism. The present data strongly support, for the first time, that human platelet lysate is a reliable and effective therapeutic source of neurorestorative factors. Therefore, brain administration of platelet lysate is a therapeutical strategy that deserves serious and urgent consideration for universal brain trauma treatment.

Received March 05, 2021. Revised April 13, 2021. Accepted May 11, 2021. Advance access publication June 4, 2021

© The Author(s) (2021). Published by Oxford University Press on behalf of the Guarantors of Brain.

This is an Open Access article distributed under the terms of the Creative Commons Attribution-NonCommercial License (<https://creativecommons.org/licenses/by-nc/4.0/>), which permits non-commercial re-use, distribution, and reproduction in any medium, provided the original work is properly cited. For commercial re-use, please contact [journals.permissions@oup.com](mailto:journals.permissions@oup.com)

- 1 Graduate Institute of Biomedical Materials and Tissue Engineering, College of Biomedical Engineering, Taipei Medical University, Taipei, 11031, Taiwan
- 2 University of Lille, Inserm, CHU Lille, U1172 - LilNCog—Lille Neuroscience and Cognition, Lille F-59000, France
- 3 Alzheimer and Tauopathies, LabEx DISTALZ, LiCEND, Lille F-59000, France
- 4 International PhD Program in Biomedical Engineering, Taipei Medical University, Taipei, 11031, Taiwan
- 5 Graduate Institute of Medical Sciences, College of Medicine, Taipei Medical University, Taipei, 11031, Taiwan
- 6 Institute of Clinical Medicine, National Yang-Ming University, Taipei, Taiwan
- 7 NeuroTMULille International Laboratory, Taipei Medical University, Taipei, 11031, Taiwan
- 8 PhD Program for Neural Regenerative Medicine, College of Medical Science and Technology, Taipei Medical University and National Health Research Institutes, Taipei, 11031, Taiwan
- 9 Graduate Institute of Neural Regenerative Medicine, College of Medical Science and Technology, Taipei Medical University, Taipei, 11031, Taiwan
- 10 NeuroTMULille International Laboratory, Univ. Lille, Lille, F-59000 France
- 11 Dementia Center, Department of Neurology, Shuang Ho Hospital, Taipei Medical University, New Taipei City, 23561, Taiwan
- 12 Neurology, School of Medicine, College of Medicine, Taipei Medical University, Taipei, 11031, Taiwan
- 13 School of Biomedical Engineering, College of Biomedical Engineering, Taipei Medical University, Taipei, 11031, Taiwan
- 14 International PhD Program in Cell Therapy and Regeneration, College of Medicine, Taipei Medical University, Taipei, 11031, Taiwan
- 15 Brain and Consciousness Research Centre, Taipei Medical University Shuang Ho Hospital, New Taipei City, 23561, Taiwan

†Present address: Institute of Clinical Medicine, National Yang-Ming University, Taipei, Taiwan

Correspondence to: Thierry Burnouf  
 Graduate Institute of Biomedical Materials and Tissue Engineering  
 College of Biomedical Engineering, Taipei Medical University  
 250 Wu-Xing Street, Taipei 11031, Taiwan  
 E-mail: thburnouf@gmail.com; thierry@tmu.edu.tw

Correspondence may also be addressed to: David Blum  
 Lille Neuroscience and Cognition, Inserm UMR-S1172, “Alzheimer & Tauopathies”  
 1 Place de Verdun, 59045, Lille Cedex, France  
 E-mail: david.blum@inserm.fr

**Keywords:** human platelet lysate; traumatic brain injury; neuroprotection; neurorestoration; neurotrophins

**Abbreviations:** CBS = cortical brain scratch; CCI = controlled cortical impact; HPPL = heat-treated human platelet pellet lysate; TBI = traumatic brain injury

## Introduction

Traumatic brain injury (TBI), resulting from road traffic accidents, sport injuries, falls, or military casualties, is a major and growing cause of disability and death worldwide, including low and high income countries, with an incidence of 69 million per year.<sup>1</sup> The pathophysiology of TBIs is very diverse and is based on the severity of the trauma. Immediate mechanical damage, resulting from direct cortical injury or intracranial pressure gradients, is followed by acute and secondary cascades of multifaceted pathological events that promote neurodegeneration and impair neuro-regeneration. Typical pathophysiological hallmarks of TBI encompass synaptic dysfunction, axonal damage, neuronal cell death, microhaemorrhages with blood leakage into the brain parenchyma, glial cell accrued activation, neuroinflammation and immune cell infiltration. Subcortical dysfunctions may also arise together with cortical lesions, lead to progressive loss of cognitive functions and favour the development of dementia.<sup>2–5</sup> In spite of these devastating socioeconomic consequences, there is no available treatment that provides effective short-term neuroprotective action or long-term neurorestorative therapy; only palliative approaches, tailor-made to the patient’s situation, are currently implemented.<sup>6,7</sup>

We reasoned that the multiple pathological events resulting from a TBI can be addressed not by a single therapeutic approach, but rather by a biotherapy capable of activating a complementary set of signalling pathways that provide synergistic neuroprotective, anti-inflammatory, antioxidative, and neurorestorative activities. Human platelet lysate, with its rich proteome, might fulfil these requirements. Indeed, human platelet lysate represents an abundant reserve of bioactive biomolecules comprising neurotrophic and angiogenic growth factors [e.g. brain-derived neurotrophic factor (BDNF), platelet-derived growth factor (PDGF), epidermal growth factor (EGF), and vascular endothelial growth factor (VEGF)], anti-inflammatory cytokines [transforming growth factor- $\beta$  (TGF- $\beta$ )], chemokines, antioxidants [superoxide dismutase (SOD), glutathione peroxidase (GPX), and catalase].<sup>8,9</sup> Platelet lysate also contains neurotransmitters (such as serotonin and histamine) that promote neurogenesis, extracellular vesicles that can serve as targeted delivery vehicles of these factors, as well as micro (mi)RNAs, to recipient cells.<sup>8–11</sup> Recent analyses have suggested that the human platelet lysate may promote cognitive functions and be of therapeutic value for the treatment of brain disorders.<sup>12,13</sup>

In the present study, we evaluated the capacity of a specific preparation of human platelet lysate, a heat-treated human

platelet pellet lysate (HPPL) to modulate and control the complex pathological events associated with TBI using a well-characterized mild controlled cortical impact (CCI) injury in mice, to mimic a concussion, as well as a new cortical brain scratch (CBS) assay, to mimic penetrating injury and brain parenchyma damage. Overall, we demonstrated, in these two models, the significant benefits afforded by both brain topical (for localized action in severe cases) and intranasal (for prolonged therapy in both moderate and severe cases) administration of the HPPL, thereby establishing a new promising and readily accessible biotherapy in clinical neuroscience for modulating short- and long-term effects of TBIs.

## Materials and methods

### Study approval and animal experiment design

All animal experiments were performed in compliance with guidelines for the welfare of animals and with the approval of an animal use protocol from Taipei Medical University (TMU) (application no. 2017–0410). In total, 177 adult male C57/BL6 mice (aged 8–12 weeks, weighing 20–30 g) were purchased from the Taiwan National Laboratory Animal Center (Nangang, Taipei, Taiwan) and housed at the TMU animal facility (Taipei, Taiwan) under a reversed light-dark cycle. Mice were used in several batches to ensure their optimal utilization.

### Bioactive compound: the HPPL

HPPL was prepared from therapeutic-grade human platelet concentrates with approval by the Institutional Review Board of TMU (TMU-JIRB no. 201802052). The platelet concentrates were obtained from healthy regular donors at the Taipei Blood Center using standardized, Taiwan FDA-licensed procedures. The donations were non-reactive for markers of blood-borne viruses (HIV, hepatitis B virus, and hepatitis C virus). When reaching the expiry date (5 days after collection), apheresis platelet concentrates were processed as described previously<sup>14,15</sup> to obtain the HPPL. Briefly, platelet concentrates were first transferred to sterile centrifugation tubes under a laminar flow hood to maintain sterility. Platelets were pelleted at 3000g for 30 min at room temperature; then the pellet surface was carefully washed with PBS to remove residual plasma proteins, and resuspended in 1/10 PBS of the initial platelet concentrate volume. Platelets were lysed to obtain the HPPL by three freeze-thaw cycles of  $-80/37^{\circ}\text{C}$ , and the mixture was centrifuged at 4500g for 30 min at  $22\pm 2^{\circ}\text{C}$  to recover the supernatant, which was heated to  $56^{\circ}\text{C}$  for 30 min. The suspension was finally cooled down to  $4^{\circ}\text{C}$ , and spun at  $10^4\text{g}$  for 15 min at  $4^{\circ}\text{C}$  to obtain the HPPL supernatant. Aliquots were prepared and stored at  $-80^{\circ}\text{C}$  until use.

### Quantification of growth factors in the HPPL by an ELISA

Concentrations of selected trophic factors including BDNF, EGF, HGF, PDGF-AB, VEGF, and TGF- $\beta$  were determined by a sandwich ELISA technique (DuoSet ELISA; R&D Systems) as described previously<sup>14</sup> following the manufacturer's protocol (a detailed description is provided in the [Supplementary material](#)).

### Cell culture

Neuroblastoma SH-SY5Y cells (ATCC CRL-2266) were used as a neuronal cell model. Cells were maintained in Dulbecco's modified Eagle medium (DMEM) supplemented with 10% foetal bovine serum (FBS, Gibco, Invitrogen), 1% non-essential amino acids (NEAAs, GE Hyclone), 100 U/ml penicillin, and 100 U/ml

streptomycin (Gibco, Life Technologies) at  $37^{\circ}\text{C}$  in a saturated humid atmosphere with 5%  $\text{CO}_2$ . Flasks (T75; Nunc, Thermo Fisher Scientific) were used for cell seeding, and when they reached 80–90% confluence, cells were gently washed with PBS before the addition of 4 ml trypsin-EDTA (Thermo Fisher Scientific). The flask was incubated for 2–3 min in an incubator to allow cells to detach. Cells were next resuspended in medium, counted, and seeded in T75 flasks or plates. SH-SY5Y cells were differentiated using  $1\ \mu\text{M}$  retinoic acid in complete growth medium (cat no. 302-79-4; Sigma) for 7 days by changing the medium every 2 days. For details of cells culture procedures, see the [Supplementary material](#).

### In vitro scratch injury

The *in vitro* scratch assay to mimic trauma was performed using differentiated SH-SY5Y neuroblastoma<sup>16</sup> cell cultures. Briefly, differentiated cells were subjected to a mechanical injury by carefully drawing parallel scratches in the cell monolayer, then treating the culture with 5% (v/v) HPPL. Closure of the wound area and axonal extensions ( $n = 3$ ) were assessed at 4 days by acquiring bright-field images using a fluorescent DMi8 microscope (Leica, Sage Vision). Cells were also stained with synaptophysin. Neurite lengths were measured using Simple Neurite Tracer software (an ImageJ plugin). Treated cells were compared to untreated cells.

### In vivo cortical brain scratch assay

A standardized *in vivo* CBS assay ([Supplementary Fig. 1](#)) as a pre-clinical translation of our *in vitro* scratch injury model<sup>17</sup> was developed to mimic penetrating injury and brain parenchyma damage that occur in moderate to severe TBIs. Animals were first anaesthetized using a combination of Zoletil<sup>TM</sup> (10 mg/kg) and xylazine (10 mg/kg). The head of an anaesthetized mouse was next fixed in a stereotaxic frame (Stoelting) using ear bars, shaved, and cleaned with 10% iodine and 75% ethanol. A midline incision ( $\sim 1$  cm long) using scissors was made to expose the skull. The soft tissue was removed from the surface of the skull and the sagittal suture, the bregma and the lambda were identified. A 4-mm diameter circle was drawn on the right parietal bone and centred between lambda and bregma with the sagittal suture tangential to the circle. A drill was used to cut along the marked circle to expose the brain. Two parallel lines at a depth of 0.6 mm and separated by 2 mm were drawn using an 18-gauge needle fixed to the stereotaxic frame. The two lines were 4 mm in length ([Supplementary Fig. 1](#)). Once the bleeding had stopped, the wound was sutured with non-absorbable sutures (nylon, 4-0, NC124) and antibiotic ointment was applied to the wound before the animal was returned to a new clean heated cage for recovery. Sham-operated (Sham) mice were subjected to a hole drill but without scratching the brain.

### Controlled cortical impact

The well-characterized CCI model was used as a reference to validate the CBS injury and determine impacts of HPPL treatment. Mice were subjected to a mild traumatic impact with a CCI device (eCCI-6.3, Custom Design & Fabrication) after Zoletil<sup>TM</sup>-induced anaesthesia. The animal head was fixed in a stereotaxic frame using ear bars. A midline incision using scissors was made on the right side to expose the skull as done for the CBS model. The sagittal suture, the bregma, and the lambda were located. A 4-mm circle in diameter was drawn over the right hemisphere and on the parietal bone at the midway i.e. centred between lambda and bregma. A hole was drilled along the marked circle ([Supplementary Fig. 1](#)). The injury was then induced using the CCI device with 3-mm tip size and after setting the following impact parameters: velocity of the actuator of 3 m/s, a deformation depth of 0.2 mm, and a dwell

time of 250 ms. The injury was initiated by impacting perpendicularly the surface of the cortex. Then, the skin was closed, and after applying antibiotic ointment to the suture to prevent bacterial infection, the mouse was moved to a heated cage to recover and allowed to live 1 or 2 weeks.

### Mouse behavioural tests

Behavioural tests were performed between 11:00 and 18:00. The equipment was carefully wiped with 75% ethanol before and after each experiment to prevent olfactory distraction. To evaluate the sensory motor function, beam and rotarod tests ( $n = 9–14$  mice/group) were performed at 3 (DPI3) and 6 days post-injury (DPI6). In addition, locomotor activity and anxiety behaviour were tested using an open-field test, and the short memory ( $n = 6$  mice per group) was assessed by a novel object recognition test. The time each animal spent to cross the beam or on the rod before falling off was recorded as its latency to fall.<sup>18</sup> The average of the three trials was calculated and recorded as the performance of the animal. For the open-field test, we evaluated the spontaneous activity of a mouse in an open-field box (60 × 60 cm) that consisted of a black wooden box under a camera. Moreover, the interaction of each animal with new and familiar objects was recorded by an automated video tracking system during 10 min. Then, the memory performance of a mouse was calculated and expressed as a discrimination index (DI) ([Supplementary material](#)).

### Administration of the HPPL

The HPPL was delivered by sequential topical and intranasal routes to address the acute phase of the injury and optimize the effect of HPPL activity over time. Approximately 30 min after CBS or CCI, and after adsorption of excess blood, 60 µl of the HPPL was slowly applied drop by drop into the wounded area before suturing the skin. The HPPL was delivered intranasally from DPI1 to DPI6.<sup>19,20</sup> Intranasal delivery was carried out as described previously.<sup>14,21</sup> Each non-anaesthetized mouse was held carefully by its ears, immobilized, and then positioned on its back with the head upright. Using a pipette, 20 µl of the HPPL was administered intranasally as four drops by alternating the nostrils. A 5-min interval was observed between each administration, for a total of three times per day. This procedure was repeated for six consecutive days, corresponding to a total volume of 420 µl per mouse. Sham and TBI-saline mice received the same volume of saline following the same intracranial and intranasal administration procedures.

### Western blot analysis for protein detection

Samples of mouse brains collected in regions of interest (ipsilateral cortex) were lysed in 200 µl lysis buffer [Tris buffer at pH 7.4 containing 10% sucrose and protease inhibitors (cat 4693132001, Complete; Roche Diagnostics)] and stored at  $-80^{\circ}\text{C}$  until used. Proteins of each sample (20 µg) were separated on 4%~12% Criterion XT Bis-Tris polyacrylamide gels (Bio-Rad) or a 4%~12% gradient GenScript Bis-Tris precast gel (GenScript) and transferred to nitrocellulose membranes. The membranes were incubated with anti-β-actin antibody (1/10 000, A5441, Sigma), anti-neuron-specific enolase (NSE; 1/1000, NA12-47, BioMol), anti-synaptophysin H-93 (1/1000, sc-9116, Santa Cruz Biotechnology), anti-Munc-18 (1/1000, M2694, Sigma), anti-SNAP25 (1/1000, Sc-376713, Santa Cruz), anti-PSD-95 (1/1000, 2507S, Cell Signaling) and anti-heat shock protein 60 (HSP60) loading control (1/10 000, ab45134, Abcam). For the complete protocol, see the [Supplementary material](#).

### Oxidative stress detection

We used the lucigenin-ECL assay to determine nicotinamide adenine dinucleotide phosphate (NADPH) oxidase-mediated superoxide radical ( $\text{O}_2^-$ ) production. At DPI7, animals ( $n = 4–5$  mice per group) were anaesthetized with Zoletil™ 50 followed by their decapitation. The cortex of each mouse was quickly dissected and kept in cold Krebs buffer (2.38 mM KCl, 1.2 mM  $\text{KH}_2\text{PO}_4$ , 118 mM NaCl, 25 mM  $\text{NaHCO}_3$ , 11 mM glucose, 1.2 mM  $\text{MgCl}_2$ , 1.2 mM  $\text{MgSO}_4$ , and 2.5 mM  $\text{CaCl}_2$ , in deionized water at pH 7.4) oxygenated (saturated with 95%  $\text{O}_2$  and 5%  $\text{CO}_2$ ) for 10 min. Fresh tissue was placed in 150 µl of buffer with 50 µl lucigenin (5 µmol/l). Using a single-tube luminometer, a baseline was first measured over 60 s. Finally, 50 µl NADPH; (100 µmol/l) was added to the test tube, and the chemiluminescence was measured over 350 s and expressed in counts per second (cps) per square centimetre ( $\text{cps}/\text{cm}^2$ ). At the end of the measurement, all samples were weighted and used to normalize cps values.

### ELISA for synaptic protein assessment

A mouse DLG4/PSD-95 ELISA kit (#E-EL-M1303), Mouse SNAP-25 ELISA Kit (#E-EL-M1106), and Mouse SYP/Synaptophysin ELISA kit (E-EL-M1105) were used to determine levels of synaptic markers according to the manufacturer's protocols (Elabscience). Brain tissue homogenates ( $n = 5–7$  mice/group) were prepared, and their protein amount was evaluated using the BCA assay kit. Synaptic protein concentrations are expressed in ng/mg of total protein.

### Gene expression analysis by quantitative PCR

RNA was extracted from collected tissues ( $n = 7–10$  mice/group) using a RNeasy Lipid Tissue Mini Kit (cat.74804, Qiagen), according to the manufacturer's protocol. NanoDrop2000 (ThermoFisher Scientific) was used to quantify the total RNA concentration. One microgram of total RNA was used to synthesize cDNA using the Applied Biosystems High-Capacity cDNA reverse-transcription kit (#4368814). Reverse transcription (RT) was run with the following programme on a StepOne™ Real-Time PCR System (ThermoFisher Scientific): 10 min at  $25^{\circ}\text{C}$ , 60 min at  $37^{\circ}\text{C}$ , 60 min at  $37^{\circ}\text{C}$ , 5 min at  $85^{\circ}\text{C}$ , and 5 min at  $4^{\circ}\text{C}$ . The obtained cDNA was stored at  $-20^{\circ}\text{C}$  prior to use in the qPCR. Validated primers were used to perform the qPCR. Reactions were prepared using 5 µl of Power SYBR Green PCR Master Mix (cat. no. 4367659, ThermoFisher Scientific), 0.1 µl of forward primer, 0.1 µl of reverse primer, 2 µl of cDNA pre-diluted 20 times, and 2.8 µl of RNase-free water for each sample. StepOne™ Real-Time PCR System was used with an amplification profile of  $50^{\circ}\text{C}$  for 12 min and  $95^{\circ}\text{C}$  for 10 min, followed by 40 cycles of  $95^{\circ}\text{C}$  for 15 s,  $60^{\circ}\text{C}$  for 30 s, and  $95^{\circ}\text{C}$  for 15 s, and then  $60^{\circ}\text{C}$  for 1 min as a step-and-hold melt curve analysis. Various inflammatory markers were screened that target astrocytic markers, microglial markers, cytokines, and chemokines, and chemokine receptors using primers described in [Supplementary Table 1](#).

### Immunohistochemistry for the histological analysis

Prior to brain sectioning, samples were removed from  $-80^{\circ}\text{C}$  and allowed to equilibrate at  $-20^{\circ}\text{C}$  for at least 30 min as the cryostat temperature. Tissues were then embedded in optimum cutting temperature medium on tissue holders. Coronal sections at 10 µm thick were cut, mounted on commercial gelatine-coated slides (Platinum PRO, adhesive glass slides), and stored at  $-80^{\circ}\text{C}$  until needed. GFAP (ref Z0334, Dako) and Iba1 (ref 019-197441, Wako) staining were performed for each sample. Fluorescence images were acquired using TissueFAXS acquisition; four sections anterior and four sections posterior to the centre of the lesion were

acquired and analysed for each animal. The intensity of immunostaining ( $n = 5/\text{group}$ ) was analysed using ImageJ (NIH) software. In addition, some slides were used to carry out a cresyl violet staining to determine the lesioned volume (Supplementary material).

### Proteomics analysis of HPPL and mice cortex

Crude HPPL and mice ipsilateral cortices ( $n = 8$ ) collected at DPI7, subjected to protein extraction in Tris-sucrose buffer were treated with acetone precooled to  $-20^{\circ}\text{C}$ , and incubated overnight at  $-20^{\circ}\text{C}$ . The ratio between the sample and acetone was 1:4. Following incubation, the mixture was spun at 15 000g for 10 min at  $4^{\circ}\text{C}$ . The supernatant was then discarded, and the protein pellet was washed twice with cold acetone in water (1:4). The sample was spun at 13 000g for 10 min at  $4^{\circ}\text{C}$  for each wash. Finally, the supernatant was discarded, and the pellet was air-dried prior to being resuspended in 6 M urea. A BCA protein assay kit was used to determine the total protein concentration, and 20  $\mu\text{g}$  of protein was sent to the proteomics core at National Taiwan University (Taipei, Taiwan) for the proteomics analysis. The list of proteins generated was next analysed using DAVID Bioinformatics Resources 6.8. A complete description of data acquisition, and proteins identification is available in the Supplementary material.

### Statistical analysis

GraphPad Prism (vers. 8.0, San Diego, CA, USA) was used to perform all analyses, and data are expressed as the mean  $\pm$  standard error of the mean (SEM) or standard deviation (SD). Multiple comparisons with a one-way ANOVA followed by Tukey's *post hoc* test was used to identify significance between groups. For the *in vitro* evaluation of the HPPL functional activity, significance was determined using Student's *t*-test. Details regarding  $n$  values, the type of comparison, and the statistical significance are indicated in the figure legends. For the western blot image analysis, ImageJ software was used for quantification.

### Data availability

The data that support the findings of this study are available from the corresponding authors on request.

## Results

### Pathophysiological development of brain lesions in CBS and CCI models of TBI

We first characterized the pathophysiological development of our new CBS model of TBI, which was designed to mimic the pathophysiological consequences of a penetrating brain injury, and compared its evolution to the CCI model, using behavioural and molecular/biochemical/histological approaches (Fig. 1A).

### CBS and CCI produce behavioural deficits in motor-dependent tasks

We evaluated general motor activity using an open-field task, at post-injury DPI3 and DPI6. There was no significant difference in the total distance travelled by mice over 10 min between the three groups (Fig. 1B). Compared to CBS, CCI mice spent a significantly longer time ( $P < 0.05$ ) in the centre of the field at DPI3 and DPI6, presumably indicating a change in anxiety behaviour. To understand the impact of CBS and CCI on motor coordination, we performed both beam and rotarod tests. The beam test revealed a significant increase ( $P < 0.005$ ) in the time spent by CBS animals crossing the elevated beam compared to the Sham animals, at

both time points (Fig. 1C, left). A significant difference between the CCI and Sham groups was essentially observed at DPI3. Further, CBS mice spent significantly less time ( $P < 0.005$ )—and a trend for CCI animals—on the rotarod at DPI3 compared to Sham animals (Fig. 1B, right), suggestive of impaired motor coordination.

### CBS and CCI promote cortical neuroinflammation

To understand the physiological events underlying CBS versus CCI injuries, neuroinflammatory gene expressions were quantified in the cortex by RT-qPCR at DPI7 (Fig. 2A). Compared to the Sham group, relative mRNA expressions of tumour necrosis factor- $\alpha$  (*Tnfa*), interleukin-1b (*Il1b*) and chemokines (*Ccl3*, *Ccl4* and *Ccl5*) in the ipsilateral cortex were found to be significantly enhanced ( $P < 0.05$ ,  $P < 0.01$ ) in CBS mice. Further, the scratch injury caused upregulation of microglial markers, such as toll-like receptors (*Tlr2* and *Tlr4*), the cluster of differentiation 68 (*Cd68*) lysosomal protein, complement component 1q (*C1q*), and triggering receptor expressed on myeloid cells 2 (*Trem2*), as well as of astroglial markers such as glial fibrillary acidic protein (*Gfap*) and vimentin (*Vim*) ( $P < 0.01$ ,  $P < 0.001$ ; Fig. 2A). In the CCI group, *Il1b*, *Ccl4*, *Cd68* and *Gfap* were significantly upregulated with similar trends for all other markers compared to Sham-treated mice. When comparing the CBS to the CCI group, we found overall significantly higher expressions of *Tlr2* and *Tlr4* receptors, *CD68*, *Trem2*, *C1q* and vimentin in the CBS group, suggesting a more severe injury in the former model (Fig. 2A). Corroborating gene expression analysis, immunohistochemical analyses of both GFAP and Iba-1 indicated cortical glial activation in both TBI models (Fig. 2B).

### Impact of CBS and CCI on cortical synaptic marker level

Next, we investigated whether the CBS and CCI injuries affected expressions of pre- and postsynaptic markers in the cortex at DPI7, using western blot analysis and dedicated ELISA. Overall, both TBI procedures led to major impairments in synaptic protein levels (Fig. 3A and B) attested by the significant decreases of synaptosome-associated protein 25 (SNAP25), synaptophysin presynaptic marker (SYP), postsynaptic density (PSD)-95 protein and mammalian uncoordinated (Munc)-18. These biochemical experiments supported similar effects between CBS and CCI models. However, as implied by the mRNA study, histological analysis of the lesion volume using cresyl violet staining highlighted that CBS procedure resulted in a larger cortical lesion than CCI (Fig. 3C).

### HPPL biotherapy for TBI

After characterizing the two TBI models and in particular, our in-house developed CBS model, we focused on determining the potential benefit of HPPL based therapy. In a first attempt, we characterized HPPL protein content before testing its potential benefits *in vitro* and then using both CCI and CBS *in vivo* models.

### Growth factor content and global proteomic analysis of HPPL

The preparation process of HPPL from the platelet concentrates is summarized in Fig. 4A. We first evaluated the concentrations of selected trophic factors including BDNF, PDGF, EGF, HGF, VEGF and TGF- $\beta$  (Fig. 4B) that were found to be similar to those described in our previous studies.<sup>14,15,22–24</sup> We extended this characterization by a global proteomic evaluation. Mass spectrometric analyses detected 1210 proteins in HPPL (Supplementary Table 2). The presence of growth factors, cytokines and antioxidants was also

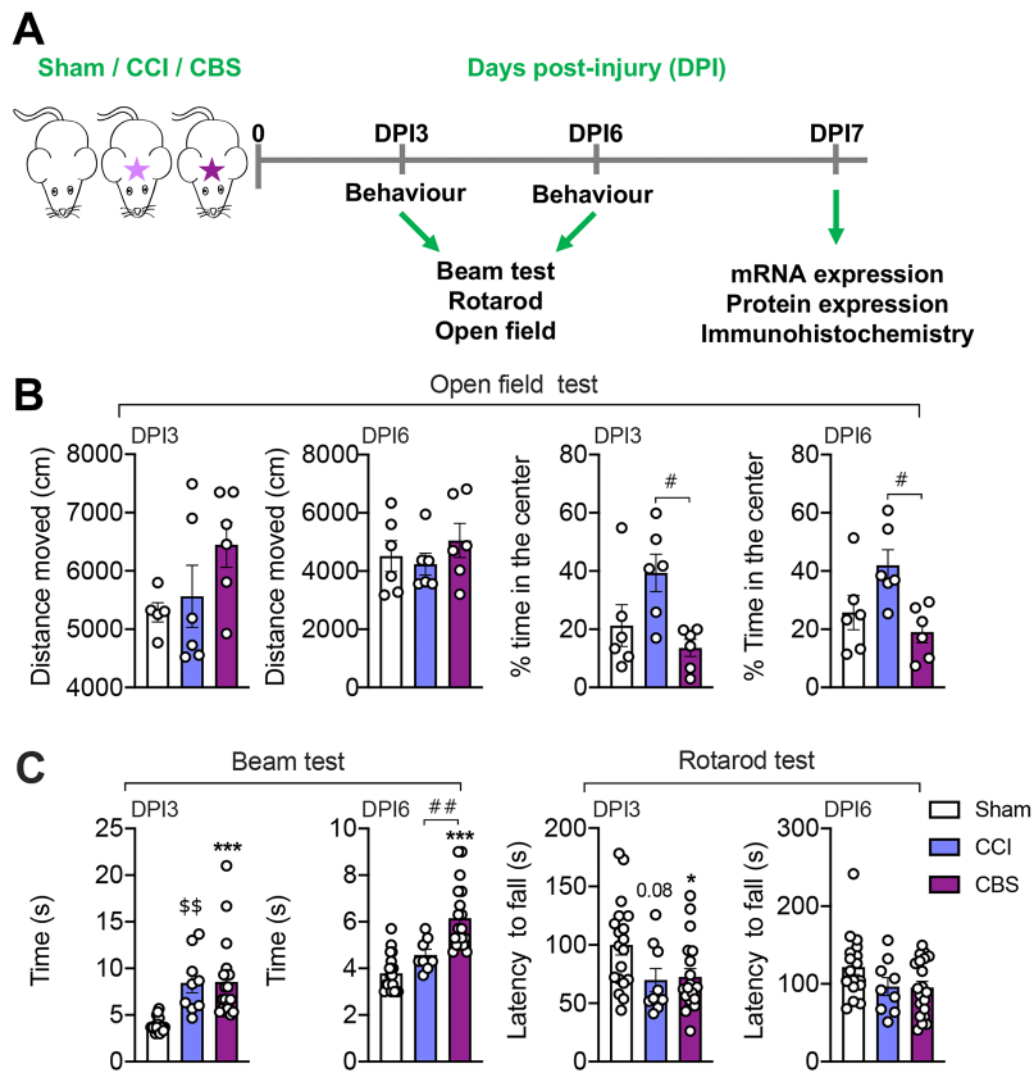


**Figure 1 Impact of TBI on motor behaviour.** Animals were subjected to sham treatment (Sham), CCI or CBS, and evaluated through open-field, beam test and rotarod tests 3 and 6 days post-surgery. (A) Schematic drawing showing the experimental design. (B) An open-field test was performed to visualize any differences in the animals' ambulation. Mice were left to freely explore a box for 10 min. The total distance and time spent in the centre of the field as an indication of anxiety-related behaviour were analysed. No difference was observed among groups for the total distance records. However, compared to CBS mice, a significant increase in the time spent by CCI mice in the centre was observed at both time points. (C) The beam and rotarod tests were performed to investigate motor coordination and balance. CCI and CBS induced significant impairment of the motor function at DPI3 as revealed by the time spent to cross a narrow beam and the latency to fall used as an indicator of motor coordination, respectively. At DPI6, only the beam test detected a significant deficit in CBS mice compared to Sham mice. Data are presented as the mean  $\pm$  SEM ( $n = 9-19$ ). \* $P < 0.05$ , \*\*\* $P < 0.001$  for CBS versus Sham;  $^{\$}P < 0.05$ ,  $^{\$\$}P < 0.01$  for CCI versus Sham;  $^{\#}P < 0.05$ ,  $^{\#\#}P < 0.01$  for CCI versus CBS, using a one-way ANOVA followed by Tukey's post hoc test.

confirmed (Supplementary Table 3) as well as other proteins previously found to exert neuroprotective activity (Supplementary Table 4). We also performed an enrichment analysis of gene ontology (GO) using DAVID Bioinformatics to delineate potential cellular processes associated with HPPL content (Fig. 4C). Among others, HPPL content was associated with Wnt signalling pathway, myelin sheath, cell adhesion, complement activation and response to reactive oxygen species (ROS)/oxidative stress.

#### Efficacy of HPPL in an *in vitro* wound closure test

We first established the functional activity and lack of cellular toxicity of HPPL using an *in vitro* mechanical trauma model of TBI. Human neuroblastoma SH-SY5Y cells were first differentiated into neuronal-like cells using retinoic acid. A monolayer of

differentiated cells was then scratched, followed by HPPL treatment. The growth of surviving cells in the wounded area was quantified by measuring the total neurite length on Day 9, 4 days post-lesion (Supplementary Fig. 2A). There was no detectable sign of toxicity due to HPPL treatment following HPPL stimulation, as we also demonstrated previously.<sup>15,23</sup> As shown qualitatively in Supplementary Fig. 2B, neurites in the scratched area were significantly longer in the HPPL treated condition compared to untreated cells. We used synaptophysin immunofluorescence to delineate and quantify neurite length in the wounded area. As shown in Supplementary Fig. 2C and D, HPPL significantly enhanced the scratch healing by stimulating the extension of cells neurites into the scratched area. By measuring the length of these neurites in the lesioned area, we illustrated the healing potential of HPPL.

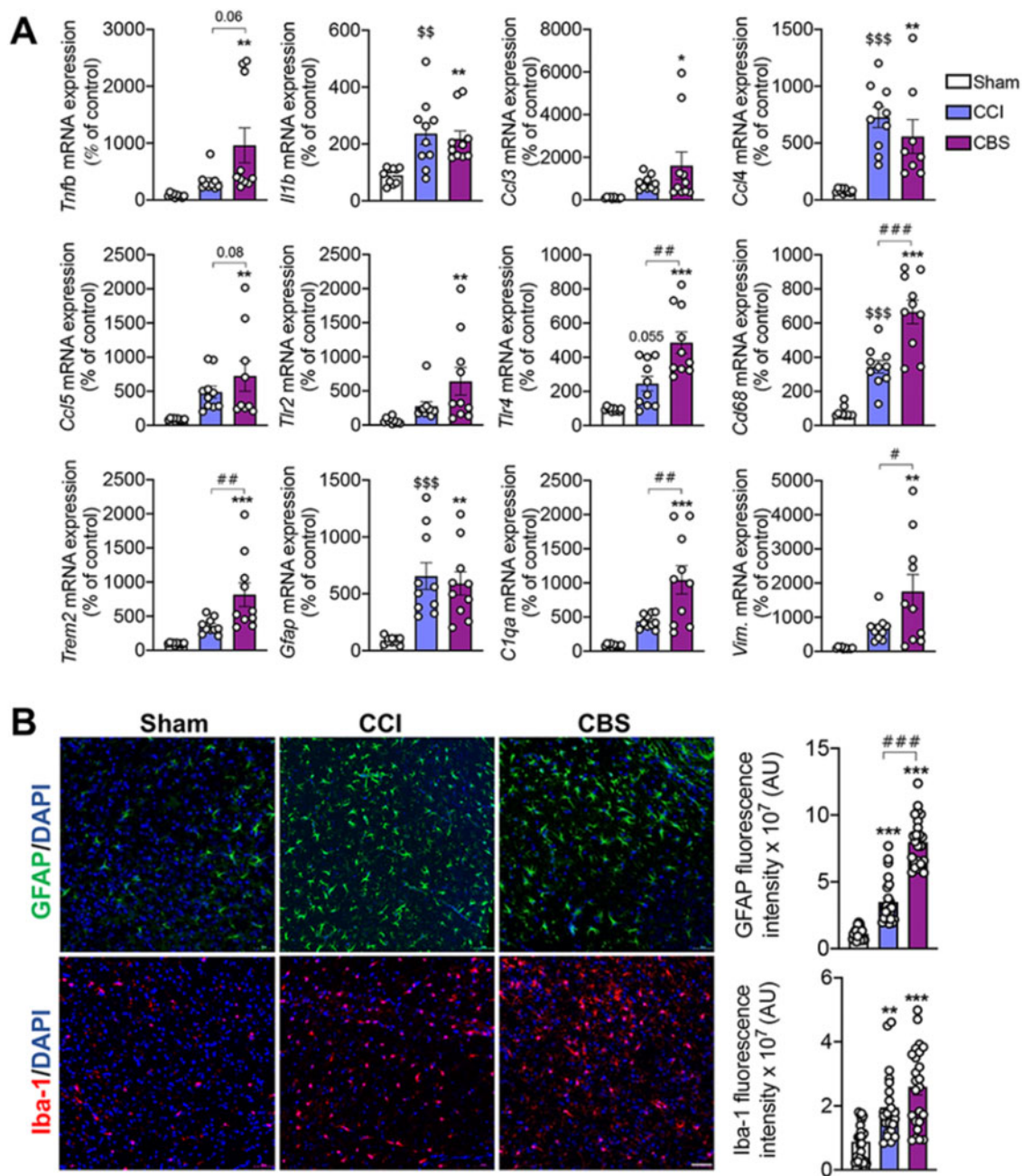


**Figure 2** Impact of TBI on cortical neuroinflammation. (A) Cytokine, chemokine and glial marker mRNA levels were evaluated in the ipsilateral cortex 7 days post-injury (DPI7). All genes tested were expressed as a percentage of sham-treated mice ( $n = 10/\text{group}$ ). (B) Immunohistochemical evaluation of GFAP and Iba-1 in the cortex of CCI and CBS animals ( $n = 5/\text{group}$ ). Scale bar =  $50\ \mu\text{m}$ . RT-qPCR and immunohistochemical data supported the development of neuroinflammation in both TBI models. Data are reported as mean  $\pm$  SEM. \* $P < 0.05$ , \*\* $P < 0.01$ , \*\*\* $P < 0.001$  for CBS versus Sham; § $P < 0.05$ , §§ $P < 0.01$  for CCI versus Sham, ## $P < 0.05$ , ### $P < 0.001$  CCI versus CBS by a one-way ANOVA using Tukey's post hoc test.

### HPPL improves motor and cognitive functions in TBI mouse models

Animals were lesioned using the CCI and CBS procedures. HPPL was delivered at the end of the surgical procedure directly on the cortex and then daily through intranasal administration until DPI6 (Fig. 5A). The beam and rotarod tests at DPI3 confirmed significantly impaired motor coordination in CCI and CBS-injured saline mice compared to Sham mice (Fig. 5B and C). In the CCI group, HPPL-treated animals spent a significantly longer time ( $P < 0.05$ ) on the rod at DPI3, compared to saline-treated mice (Fig. 5C). Moreover, in CBS mice, HPPL administration significantly decreased the time

spent to cross the beam test at DPI3 ( $P < 0.001$ ) and DPI6 ( $P < 0.01$ ; Fig. 5B) and enhanced latency to fall increased compared to saline-treated animals ( $P < 0.05$ ; Fig. 5C). In addition, a longer-term investigation (DPI14) of the effects of HPPL on short-term memory deficits using the novel object recognition test evidenced a significant memory alteration of the discrimination index between saline-treated mice and Sham animals in both TBI models ( $P < 0.001$ ; Fig. 5D). HPPL delivery successfully increased the discrimination index in the CBS group ( $P < 0.05$ ). The same trend was seen in HPPL-treated CCI animals, even though statistical significance difference was not achieved (Fig. 5D). Thus, besides motor improvement, HPPL also improved longer term memory alterations in TBI models.

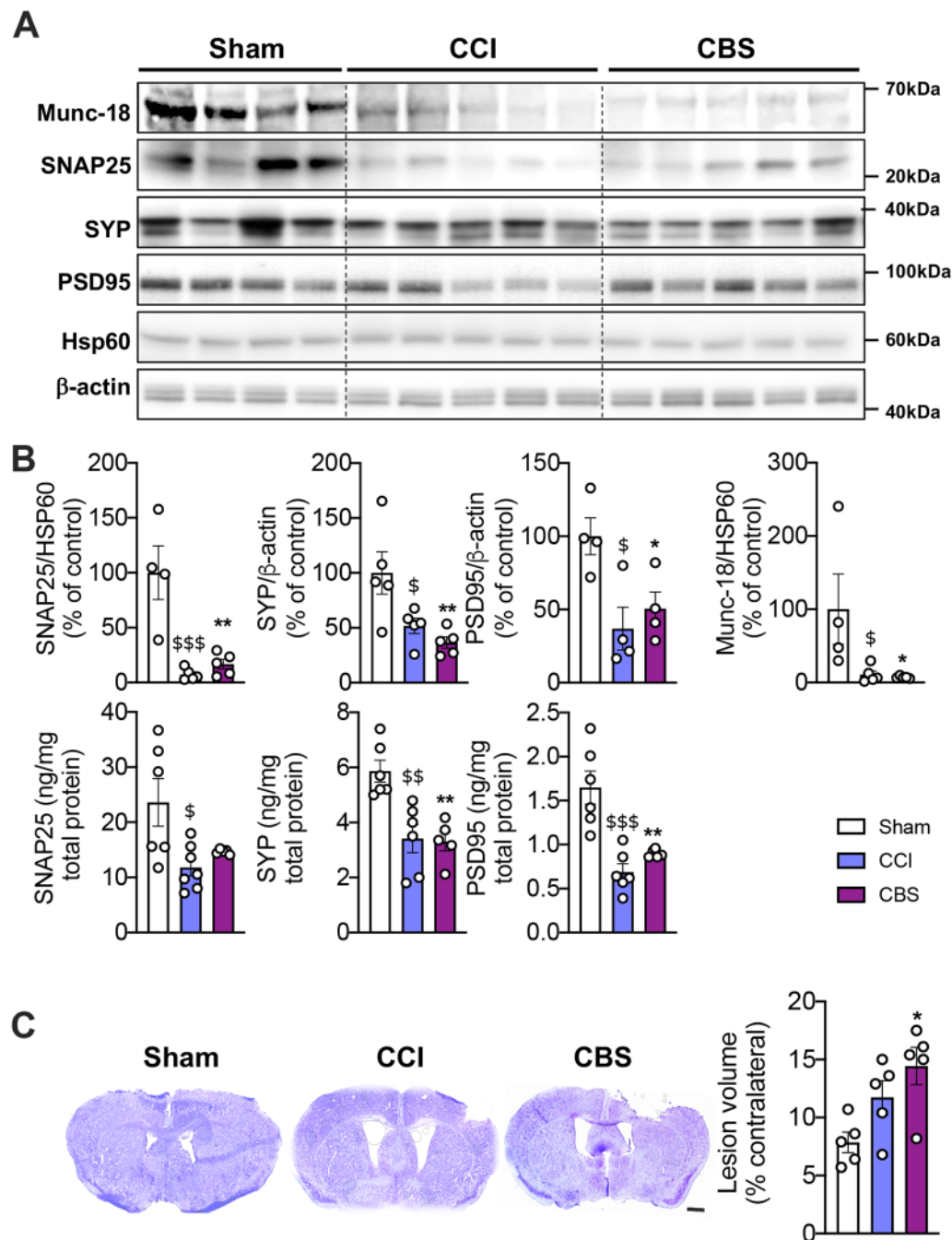


**Figure 3** Impact of TBI on cortical synaptic markers. (A) Western blot analysis of ipsilateral cortex at DPI7. (B) Densitometric analysis of protein expression (top). ELISA determination (bottom). Data support the significant loss of synaptic proteins 7 days post-injury. (C) Cresyl violet staining has been used to evaluate the lesion volume in TBI animals. Data are expressed as the mean ± SEM by a one-way ANOVA with Tukey’s post hoc test; n = 4–7 mice per group. \*P < 0.05, \*\*P < 0.01, for CBS versus Sham; \$P < 0.05, \$\$\$P < 0.01, \*\*\*\*P < 0.001 for CCI versus Sham. Scale = 250 μm.

### HPPL mitigates cortical neuroinflammation in TBI mouse models

The ability of HPPL administration to impact neuroinflammation triggered by the CBS and CCI procedures was tested by examining differential gene expressions, compared to saline treatment. As expected, and according to data in Fig. 2, the markers studied were found to be upregulated in the cortex of TBI-saline animals compared to Sham animals at DPI7 (Fig. 6A and B). In CCI animals, following HPPL administration, we observed a significant (P < 0.05–0.001) downregulation of *Il1b* and chemokines (*Ccl3*, *Ccl4*,

*Ccl5*) as well as of *Tlr4*, *Cd68*, *Trem2*, *Vim*, and *Gfap* glial markers compared to the saline-treated group (Fig. 6A). In the CBS model, HPPL administration led to decreased expression of *Tnfa*, *Ccl4*, *Tlr4*, *Cd68*, *Trem2* and *Gfap* (P < 0.05–0.001) compared to saline-treated animals (Fig. 6). Expression of *Il1b*, *Ccl3*, *Ccl4*, *Ccl5*, *Tlr2*, *C1qa*, and *Vim* were also decreased but without reaching significance. In addition, GFAP and Iba-1 immunofluorescence showed decreases in their levels following HPPL administration in both TBI groups (P < 0.05–0.001; Supplementary Fig. 3A and B), suggestive of reduced neuroinflammatory processes, in line with mRNA studies (Fig. 6).

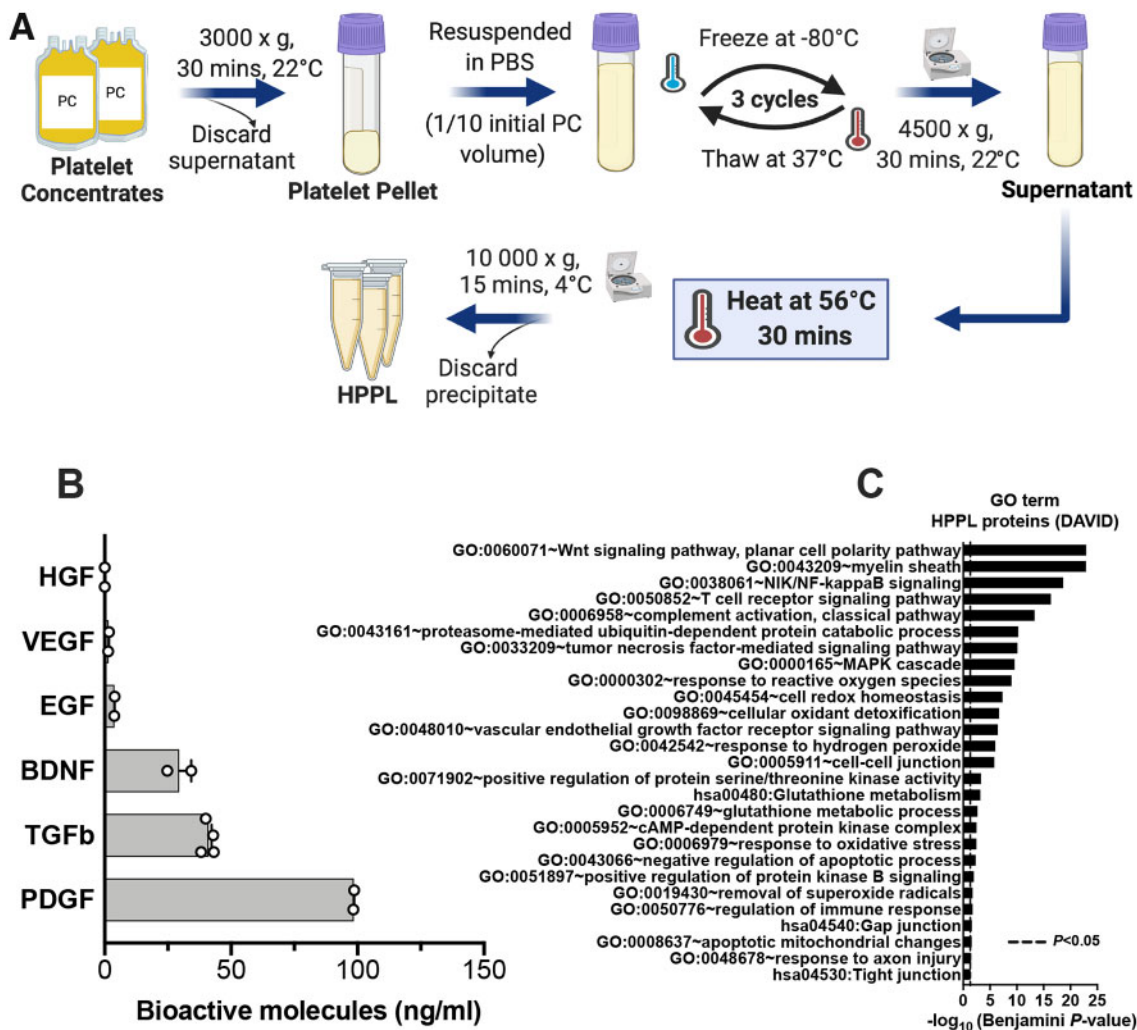


**Figure 4** Characterization of HPPL. (A) HPPL preparation procedure. (B) ELISA dosage of several trophic factors in the HPPL: hepatocyte growth factor (HGF), vascular epithelial growth factor (VEGF), epidermal growth factor (EGF), brain-derived neurotrophic factor (BDNF), transforming growth factor -  $\beta$  (TGF- $\beta$ ), and platelet-derived growth factor subunit-AB (PDGF-AB). The HPPL consisted of a pool of three batches ( $n = 3$ ). Values are expressed as the mean  $\pm$  SEM. (C) Proteomic analysis of the HPPL using LC-MS/MS. The panel represents GO analysis with relevant biological processes represented by the identified proteins. As expected, the HPPL contained detectable amounts of growth factors and a plethora of bioactive molecules (1210 proteins were identified in this specific preparation).

### HPPL mitigates synaptic impairments in the cortex of TBI mice

As expected, animals from CCI and CBS-saline groups exhibited a significant ( $P < 0.05$ – $0.001$ ) loss of pre- (SNAP25, Munc-18, SYP) or postsynaptic (PSD-95) proteins compared to Sham animals (Fig. 7A–D). Higher expressions of synaptophysin (ELISA) and PSD-95 (western blot analysis) and Munc-18 were observed in the cortex of CCI + HPPL-treated animals compared to saline-treated mice. In the CBS model, levels of SNAP-25, synaptophysin (ELISA) and Munc-18 levels were significantly higher ( $P < 0.01$ ) in the HPPL-treated group compared to the saline group. Overall, these data indicated that, in both the CCI and CBS models, HPPL treatment mitigated the loss of cortical synaptic proteins.

### HPPL induces a reduction in reactive oxygen species levels and enhances antioxidant defence in the cortex of TBI mice

Oxidative stress worsens neuronal damage after a TBI. We therefore investigated whether HPPL treatment potentially attenuated

oxidative stress by focusing on the mRNA expression of enzymes involved in the antioxidant response. RT-qPCR evaluations (Supplementary Fig. 4A and B) indicated a significant ( $P < 0.05$ – $0.001$ ) increase in the expression of *Gpx1*, *Ho-1* (*Hmox1*) and *Nqo1* in HPPL-treated CCI animals compared to saline-treated animals. In the CBS group, HPPL treatment led to a significant increase of *Ho-1*, *Sod1*, *Gpx1*, *Sod2*, and *Nqo1* followed the same trend without reaching statistical significance. Additionally, using a lucigenin-enhanced chemiluminescence assay, we determined NADPH oxidase-mediated superoxide radical ( $O_2^-$ ) production. A significant 3-fold increase ( $P < 0.001$ ) of NADPH oxidase-dependent superoxide ion production was found in the ipsilateral cortex of CBS mice compared to Sham mice, that returned to basal level in HPPL-treated animals ( $P < 0.01$ ; Supplementary Fig. 4B).

### Proteomic cortical changes induced by HPPL in TBI models

We finally performed a proteomics analysis to determine the global impact of HPPL on TBI pathophysiology using a non-driven hypothesis analysis. Samples derived from the cortices of DPI7 Sham,

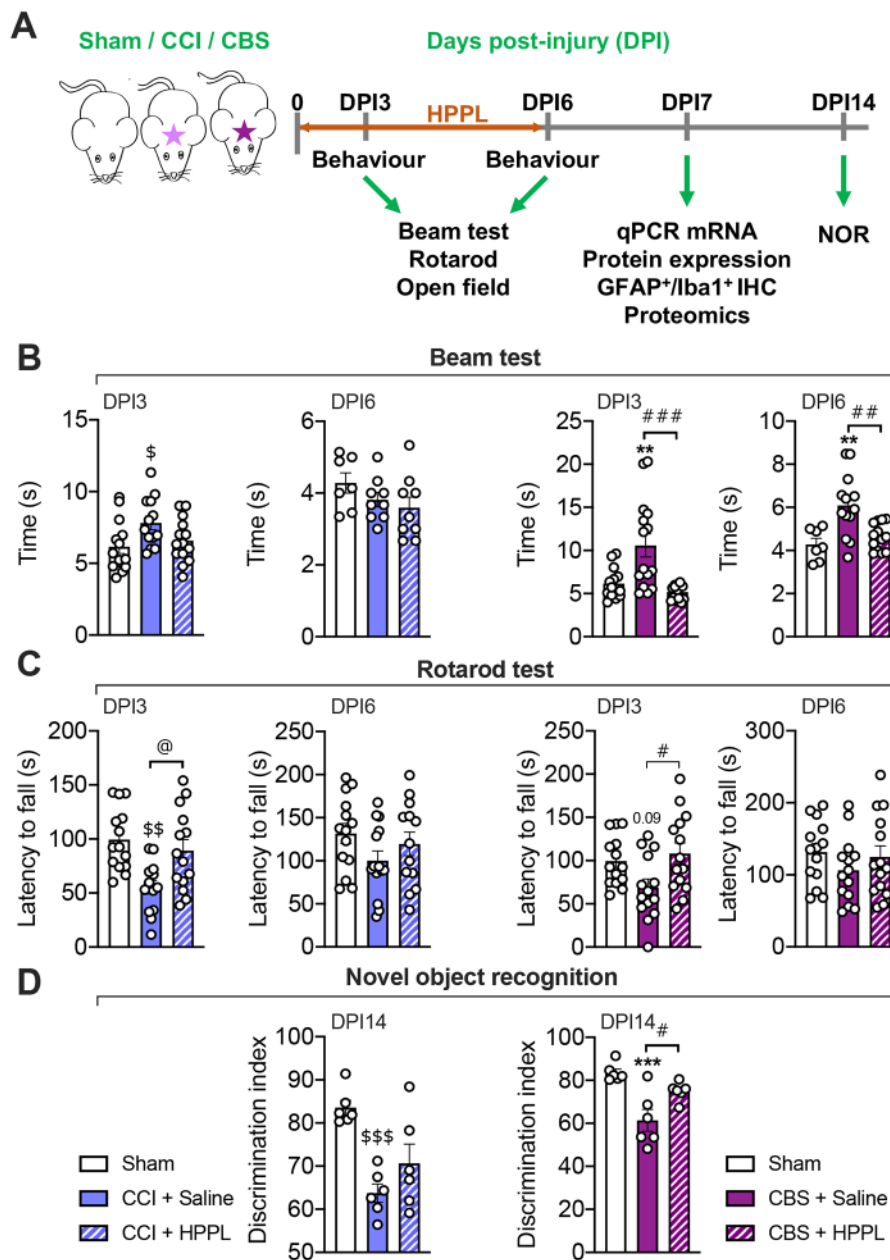


**Figure 5 HPPL improves motor and cognitive functions in TBI mouse models.** Mice were subjected to either a CCI injury, CBS injury, or sham surgery (Sham). HPPL (60  $\mu$ l) or vehicle alone was applied to the injured area, once the bleeding had stopped. A 60- $\mu$ l intranasal administration was then carried out daily for 6 days. (A) Experimental timeline. (B) The beam test was performed at DPI3 and DPI6 to investigate motor coordination and balance. (C) The rotarod test performed at DPI3 and DPI6. Data are presented as the mean  $\pm$  SEM ( $n = 9-14$  per group). Significance was determined by ANOVA followed by Tukey's *post hoc* analysis. CCI model:  $^{\$}P < 0.05$  or  $^{\$\$}P < 0.01$  for CCI versus Sham;  $^{\textcircled{a}}P < 0.05$  for CCI-saline versus CCI-HPPL. CBS model:  $^{**}P < 0.01$  CBS compared to Sham;  $^{\#}P < 0.05$  or  $^{\#\#}P < 0.01$ ,  $^{\#\#\#}P < 0.001$  for CBS-saline versus CBS-HPPL. (D) Six mice per group were also tested for novel object recognition at DPI14. The discrimination index estimated the ability of an animal to distinguish a novel object from a familiar one. Data are presented as the mean  $\pm$  SEM and an ANOVA followed Tukey's *post hoc* analysis.  $^{\$\$\$}P < 0.001$  for CCI-vehicle versus Sham.  $^{***}P < 0.001$  for CBS versus Sham,  $^{\#}P < 0.05$ , CBS-HPPL versus CBS-saline.

CCI and CBS mice treated with either saline or HPPL were analysed. First, we compared the cortical proteins impaired by both TBI procedures compared to Sham animals. The changes in protein levels were considered significant with fold change  $> 2$  (upregulated) or  $< 0.5$  (downregulated). As shown in Fig. 8A, TBI procedures induced change in a large number of cortical proteins: 634 for CCI and 817 for CBS. Notably, most of the changes were due to protein upregulations: 503 of 634 changes (79.3%) in CCI animals and 761/817 (93.1%) in CBS animals. Three hundred and forty-three of those were found upregulated in both the CCI and

CBS groups (Fig. 8A). Functional annotation identified that these 343 common upregulated proteins found in both TBI models belong to pathways related, for instance, to exosomes, focal adhesion, mitochondria, cytoskeleton and lipid metabolism (Supplementary Fig. 5A). Interestingly, according to our above-mentioned data, several markers, such as CD44, vimentin and GFAP, were found to be highly upregulated, suggestive of astrogliosis as well as microglial C1q protein, involved in synaptic loss. The list of the common upregulated proteins is provided in Supplementary Table 5.

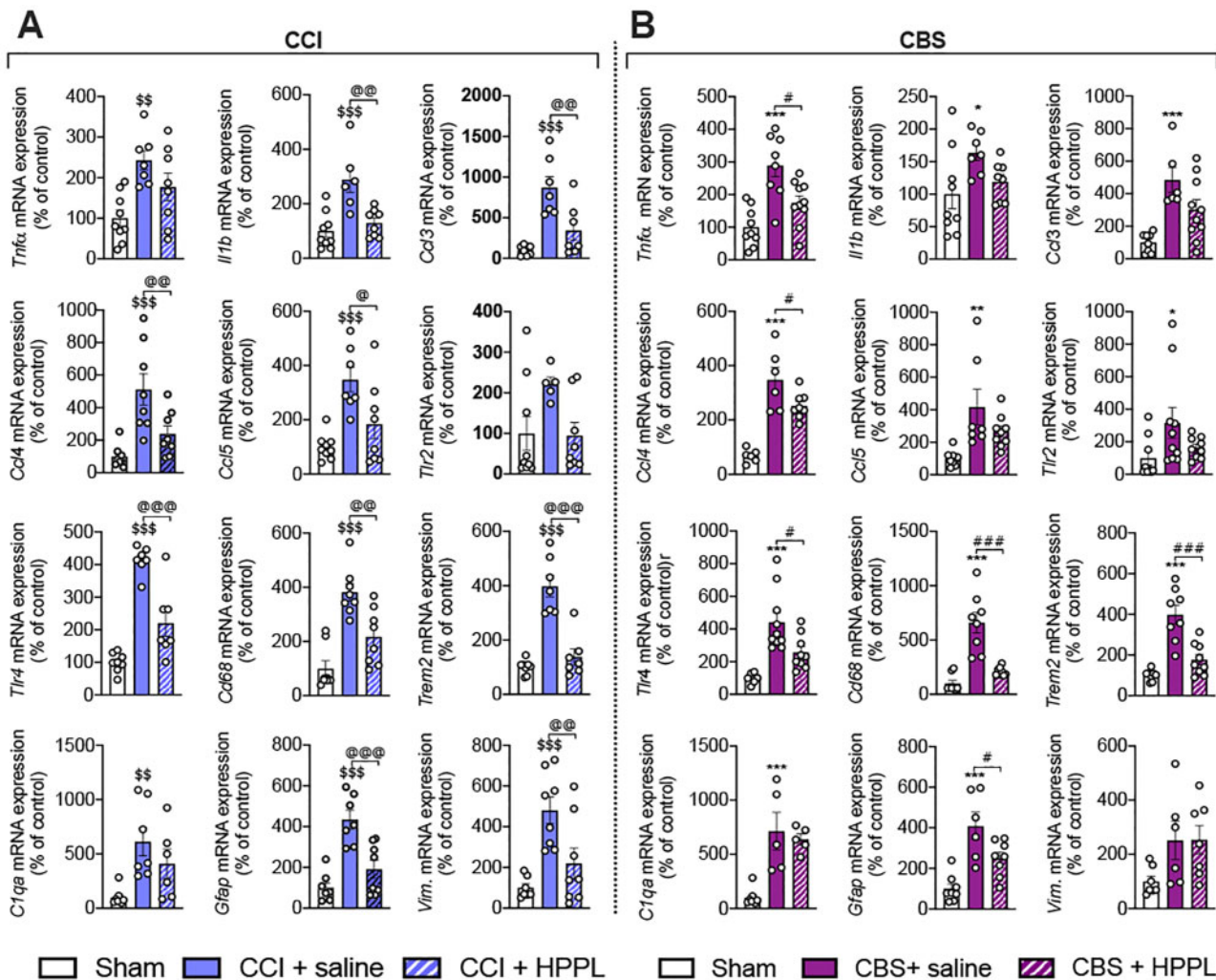


**Figure 6** HPPL mitigates cortical neuroinflammation in TBI mouse models. Mice were injured by CBS or CCI, then treated immediately after the injury with either 60  $\mu$ l topical HPPL or vehicle, followed by a daily intranasal administration until DP16. One-week post-injury, mice were sacrificed, the ipsilateral cortex was dissected, and cytokine, chemokine, and glial marker mRNA levels quantified by RT-qPCR. Transcriptional analysis of inflammatory markers ( $n = 7-8$  mice per group) in the CCI model (A) and the CBS model of TBI (B). As expected, most of the markers were upregulated in saline-treated mice compared to sham-treated mice. HPPL administration significantly downregulated several of the inflammatory markers raised by CCI or CBS. Data are reported as the mean  $\pm$  SEM;  $^{\$}P < 0.01$ ,  $^{\$ \$ \$}P < 0.001$  for CCI-vehicle versus Sham;  $^{\text{C}}P < 0.05$ ,  $^{\text{C}^{\text{C}}P} < 0.01$ ,  $^{\text{C}^{\text{C}^{\text{C}}P} < 0.01$  for CCI + saline versus CCI + HPPL;  $^*P < 0.05$ ,  $^{**}P < 0.01$ ,  $^{***}P < 0.001$  for CBS versus Sham,  $^{\#}P < 0.05$ ,  $^{\#\#}P < 0.01$ ,  $^{\#\#\#}P < 0.001$  CBS + saline versus CBS + HPPL, by a one-way ANOVA followed by Tukey's *post hoc* test.

Importantly, when we compared the cortical proteins modulated by the HPPL treatment in both TBI models, we observed that most of the changes observed were due to protein downregulation. Indeed, as shown in Fig. 8B, HPPL induced change in 446 proteins in the CCI model, 337 (75.5%) being downregulated; in the CBS model, HPPL induced change in 1708 proteins, 1635 (95.7%) being downregulated. Two hundred and thirty-two were found to be downregulated by HPPL in both the CCI and CBS models (Fig. 8B). Functional annotation identified that several of the pathways downregulated by HPPL were common to pathways found to be upregulated by TBI (Supplementary Fig. 5B, red bars). In other words, HPPL reversed several pathways promoted by both CCI and CBS and related to transport, postsynaptic density, mitochondria or lipid metabolism. Moreover, we sought for a particular signature upregulated in both TBI models, which was reversed and therefore downregulated by the HPPL treatment. As shown in Fig. 8C, we found a group of 41 proteins fulfilling this criterion that we analysed using STRING (functional protein association networks tool, <https://string-db.org>). As shown in Fig. 8D, some of these 41

proteins belong to functional networks associated with translation and fatty acid biosynthesis

Finally, considering the links between both TBI models and neuroinflammatory processes, we also compared our proteomics data to two recent uncovered (transcriptomic) signatures of disease-associated microglia (DAMs)<sup>25</sup> and astrocytes (DAAs).<sup>26</sup> Among the 471 upregulated DAM markers, signing pathological phenotype of microglia, 25 and 38 were found to be upregulated in the cortex of CCI and CBS animals, respectively (Supplementary Fig. 6A). Among these, two and 23 were downregulated, respectively, in HPPL-treated animals. Importantly, most of these downregulated 23 proteins belonged to the STRING network related to ribosomes (Supplementary Fig. 6B), in accordance with the network uncovered in Fig. 8D. Moreover, among the 239 upregulated DAA markers, 44 and 38 were upregulated in the cortex of CCI and CBS animals, respectively (Supplementary Fig. 6A). Among them, two and 15 markers were downregulated in HPPL-treated animals, respectively. HPPL therefore mitigated DAM and DAA changes triggered by brain damage, particularly in

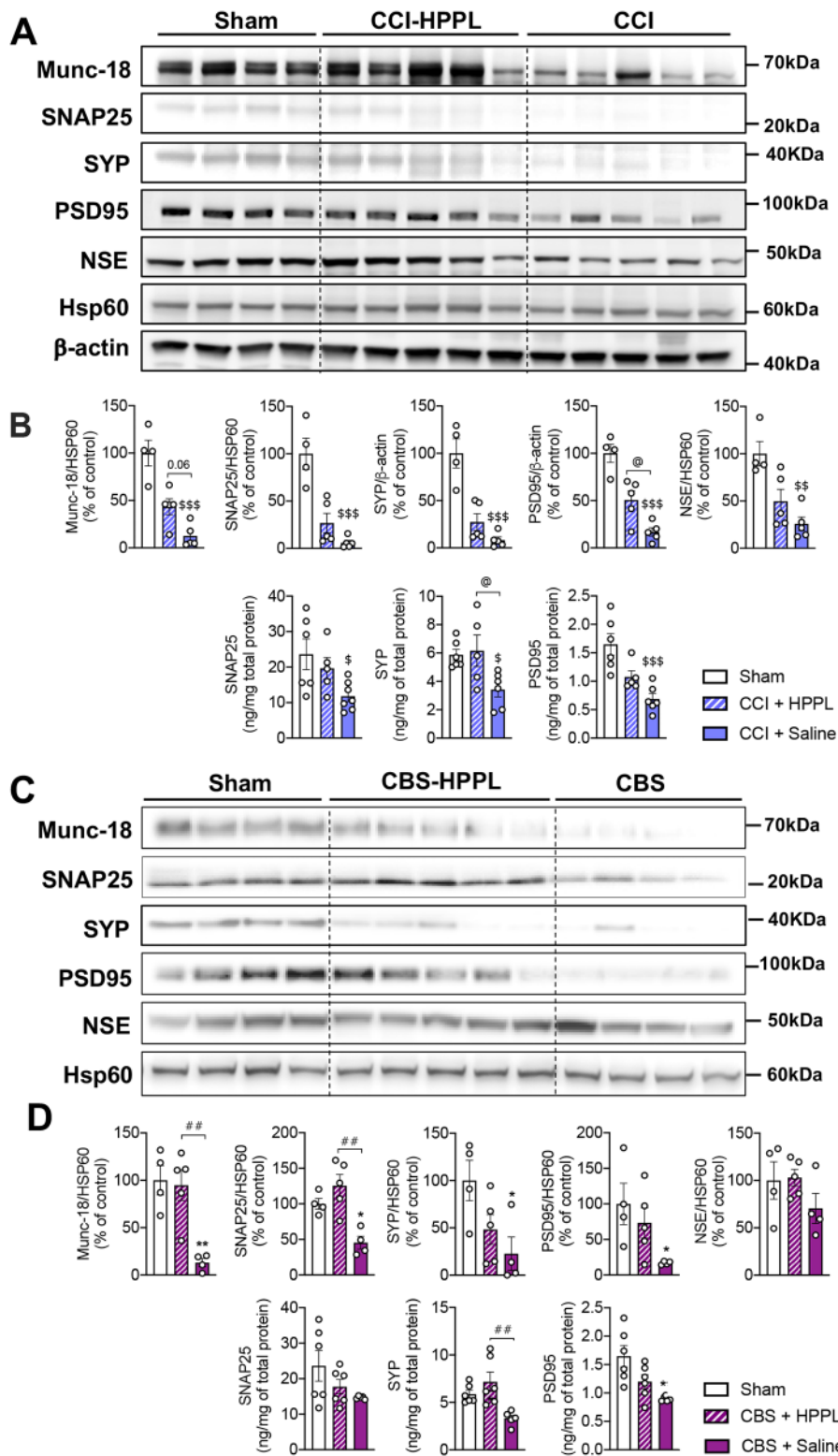


**Figure 7** HPPL mitigates synaptic impairments in the cortex of TBI mice. Western blot analysis of synaptic proteins at DPI7 in the CCI (A) and CBS (C) models. Densitometric analysis showing the differential expression of the tested proteins (B and D, top). ELISA analysis of three synaptic proteins (B and D, bottom). The results confirmed loss of synaptic proteins following TBI and demonstrated the protection by HPPL. Data are expressed as mean  $\pm$  SEM. \* $p < 0.05$ , \*\* $p < 0.01$ , \*\*\* $p < 0.001$  for CCI versus Sham, <sup>Ⓢ</sup> $p < 0.05$ , <sup>ⓈⓈ</sup> $p < 0.01$  for CCI versus CCI + HPPL. \* $p < 0.05$ , \*\* $p < 0.01$  for CBS versus Sham; # $p < 0.05$ , ## $p < 0.01$  for CBS versus CBS + HPPL by a one-way ANOVA followed by Tukey's post hoc test.

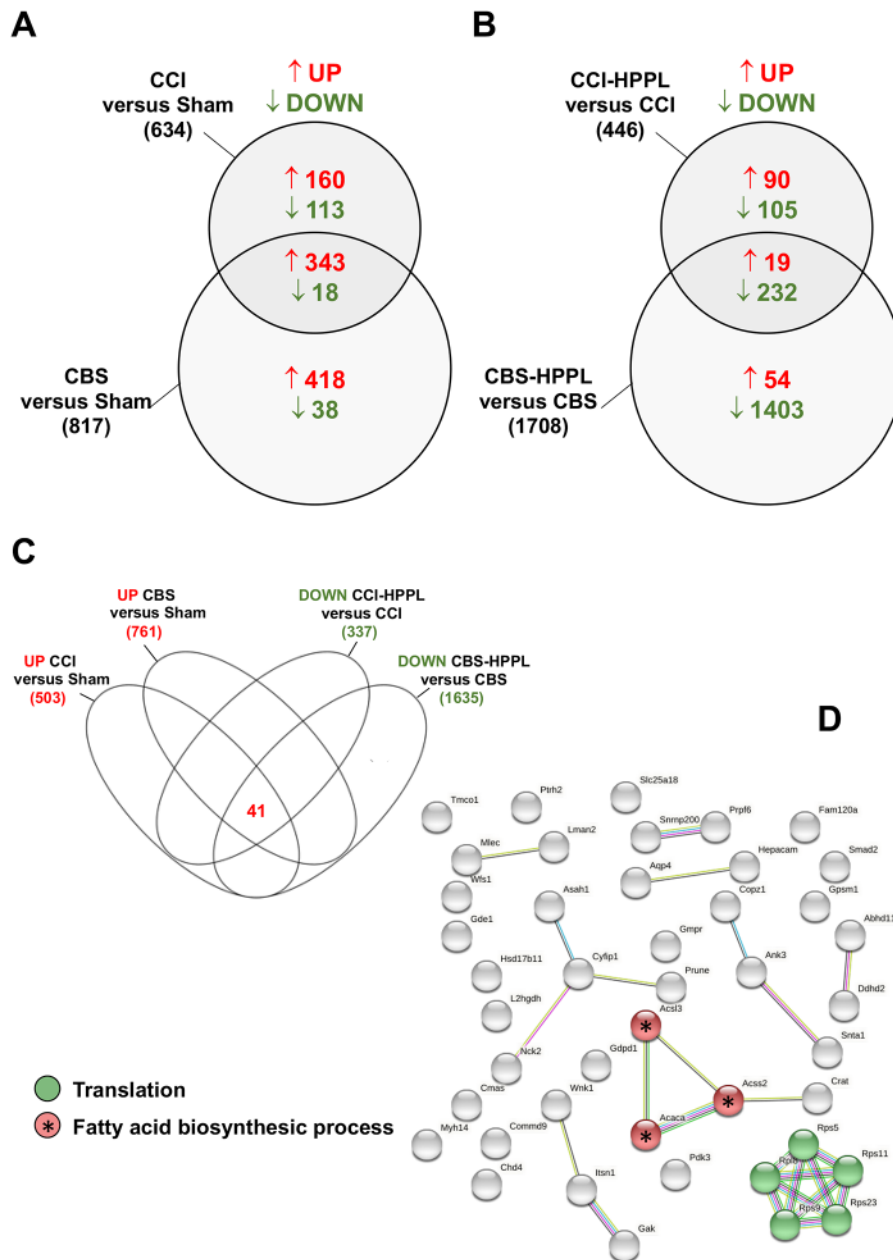


**Figure 8** Quantitative proteomics highlights differentially regulated proteins following CBS and CCI injury models as well as the impact of the HPPL treatment. To investigate the effect of HPPL on the overall expression of proteins in lesioned cortical tissues, a proteomics analysis was performed with cortical tissues from treated, untreated, and sham-operated (Sham) mice ( $n = 8$ ). The tissue was collected at 7 days post-injury. (A) The number of dysregulated proteins (red = number of upregulated proteins, green = downregulated) following the TBI procedures. Venn diagram of differentially expressed proteins in CCI versus Sham and CBS versus Sham indicates that the majority of the differentially expressed proteins are upregulated in the two models of TBI, and 343 proteins among them are in common. (B) Venn diagram of differentially expressed proteins in CCI-HPPL versus CCI and CBS-HPPL versus CBS. The results indicate that HPPL biotherapy successfully reversed the expression of 337 proteins in CCI mice, and 1635 in CBS. Among the proteins downregulated by HPPL, 232 were common to CCI and CBS. (C) Venn diagram showing proteins upregulated in both CBS versus Sham and CCI versus Sham, and downregulated in both CCI-HPPL versus CCI, and CBS-HPPL versus CBS. There were 41 proteins in common between the four conditions. (D) Protein-Protein Interaction (PPI) network analysis performed using STRING database highlighting proteins initially upregulated following CCI and CBS injury and downregulated by HPPL treatment. Two functional networks were found with this analysis: fatty acid biosynthesis process and translation.

the CBS model. These data further highlight the overall ability of HPPL to reduce the neuroinflammatory load, notably in the most severe conditions. Overall, our proteomic data highlight that HPPL is prone to reverse several pathological cortical pathways induced by two TBI procedures that may favour synaptic degeneration, neuroinflammation and ultimately behavioural impairments.

## Discussion

TBIs have a complex multifaceted progressive pathology, potentially leading to chronic long-term cognitive defects<sup>4,5</sup> for which treatments are still lacking. Excessive neuroinflammation, development of oxidative stress, and neuroendocrine dysfunctions are among key contributors to neuronal deaths and disabilities

associated with TBI. Promoting neuro-regeneration and restoration of neurological functions in an injured brain remains extremely challenging.<sup>27</sup> In the search for effective treatments, several recent lines of evidence suggest that platelet proteome may emerge as a potent novel biotherapy for treating neurological disorders<sup>12,13</sup> based on its abundant contents of pleiotropic neurotrophic and angiogenic factors, among other active biomolecules.<sup>8</sup> Herein, for the first time, we examined the efficacy of the HPPL applied topically and subsequently delivered intranasally to exert neuroprotective and neurorestorative actions following a TBI in mice. With this goal in mind, we used two *in vivo* models of TBI based on different triggers and outcomes, in order to capture potential benefits of the HPPL in a context of unpredictable pathophysiological events associated with this very diverse and complex pathology. The well established CCI model was used to mimic a mild TBI resulting from a concussion,<sup>28</sup> whereas we developed and characterized a novel *in vivo* scratch injury assay of the cortex (CBS) to capture the pathophysiological cascade of events associated with a penetrating trauma. Indeed, one single experimental model is unable to fully mimic the TBI pathophysiology, and several experimental models are therefore needed to address the underlying complex disease mechanisms. Using the same approach as that used in the *in vitro* scratch assay, we developed a simple and affordable *in vivo* scratch injury model for drug screening and to address the multifaceted nature of TBIs. The CBS model was performed by exposing the dura mater and precisely scratching the exposed brain with two controlled parallel injuries for optimal standardization. The CBS injury triggered important pathophysiological cortical changes including glial activation, oxidative stress, and synaptic impairments ultimately translated into motor deficits but also long-term memory impairment (Fig. 6D). The overall detrimental pathophysiological and behavioural effects of CBS compared to Sham animals were obvious, and, more pronounced than those resulting from mild injury induced by the controlled pneumatic CCI impactor, as attested by the larger cortical lesion or proteomic changes. As targeted, both the CBS and CCI models provided well-identified quantitative biochemical and motor function readouts to characterize the functional capacity of HPPL treatment to modulate the TBI pathology.

The HPPL used in this study was prepared from clinical grade platelet concentrates and characterized by ELISA and an LC/MS proteomics analysis. These analyses showed the presence of classical neurotrophins and neuroprotective cytokines including BDNF, EGF, HGF, VEGF, PDGF, a neuron and glial growth regulator (glia maturation factor beta),<sup>29</sup> less known neuroprotective factors (TIMP-1, Neurabin-2 etc.), antioxidative agents (catalase, glutathione S-transferases, SOD, guanase),<sup>30</sup> and anti-inflammatory molecules TGF- $\beta$ , fibroblast growth factor (FGF), insulin-like growth factor (IGF), etc. This is in line with previous characterization of the HPPL by ELISA that established its high contents of neurotrophic, angiogenic, and anti-inflammatory growth factors such as PDGF, BDNF,  $\beta$ -FGF, VEGF, and TGF- $\beta$ 1.<sup>14,15,22,23</sup> Here, we also provide a more extensive characterization of HPPL using proteomics. As revealed by the GO term analysis, bioactive proteins in the HPPL are involved in several biological processes including vascular regeneration, wound healing, metabolic processes, immune response, vesicle-mediated transport, protein transport, etc. This complex proteome can therefore exert unique potent synergistic functional activities contributing to neuroprotection and neurorestoration,<sup>12</sup> consistent with previous reports.<sup>31–33</sup> In addition, the HPPL chemical composition has recently been published<sup>24</sup> and we have found that it contains over  $10^{11}$  extracellular vesicles/ml (unpublished results). Extracellular vesicles derived from platelets may exert important functional activities<sup>11</sup> and may contribute to diffusion of neurotrophic factors and repair of damaged cells in

the brain.<sup>34,35</sup> We are conducting further studies to determine the possible contribution of extracellular vesicles to the functional activity of HPPL. In addition, the efficacy of HPPL may also reside in the presence of various neurotransmitters, including GABA, serotonin, glutamate, or dopamine, which are known to be stored in platelets, as reviewed recently,<sup>13</sup> and, like serotonin, to decrease oxidative stress.<sup>36</sup>

The functionality of HPPL was first evaluated in an *in vitro* TBI model using differentiated neuronal cells. HPPL treatment efficiently stimulated neurite outgrowth as revealed by the extension of cells into the wounded area compared to untreated cells. These data confirm our previous studies using non-differentiated neuronal cells, where HPPL treatment led to morphological changes reflective of their differentiation as well as enhanced expression of the  $\beta$ 3-tubulin marker of differentiated neurons.<sup>15</sup> Altogether these *in vitro* data provided evidence of the capacity of HPPL to trigger neuronal differentiation and repair TBI-like injuries, with reorganization of neuronal branching and building of new synapses, which promote functional recovery.<sup>37</sup> These data encouraged us to evaluate the HPPL in TBI animal models. In both *in vivo* TBI models evaluated herein, sequential treatment with 60  $\mu$ l of topical HPPL deposited in the injured cortex area, first, followed by six daily pulses of 60  $\mu$ l intranasal delivery provided potent functional effects reflected by the significant downregulation of multiple markers of glial response and neuroinflammation in the cortex. Neuroprotective and neurorestorative capacity of such HPPL treatments were suggested by changes in the levels of pre- and postsynaptic markers. Furthermore, an antioxidative effect of HPPL was found in the ipsilateral cortex as illustrated by stimulation of the transcription of the antioxidant enzymes HO-1, NQO-1, and GPx, which are also known as detoxification agents.<sup>38</sup> This finding also provides a link to the nuclear factor-erythroid 2-related factor 2 (Nrf2), which promotes the transcriptional activation of HO-1, GST, NADPH, NQO-1 and SOD.<sup>39</sup> Therefore, the antioxidative effect of HPPL may likely be due to a direct supply of bioactive molecules leading to upregulation of antioxidant enzymes or through activation of the Nrf2 pathway, which is known to be involved in antioxidant actions.<sup>40,41</sup> These interesting results suggest that the HPPL can prevent secondary damage in the early-stage post-injury by protecting cells from lipid peroxides.

Our proteomic studies highlight the diversity of pathways associated with the HPPL restorative potential, fitting perfectly with the concept of a multitargeting biotherapy providing synergistic neuroprotective, anti-inflammatory, antioxidative, and neurorestorative activities. We performed two proteomic studies: the analysis of HPPL itself as well as the analysis of cortical changes promoted by the HPPL in the TBI context. On the one hand, the GO term annotation arising from the HPPL analysis supported the HPPL proteome's involvement in several biological and molecular functions including Wnt signalling pathway, myelin sheath, T-receptor signalling pathways, response to reactive oxygen species, etc. For instance, the Wnt pathway is associated with the regulation of critical biological processes including neurogenesis, synaptogenesis, neuronal plasticity, synaptic plasticity, angiogenesis, vascular stabilization, and inflammation.<sup>42,43</sup> This pathway was also reported to be involved in neuroprotection and neurorestoration following TBI,<sup>44–46</sup> and therefore could explain the ability of HPPL to support differentiation of neuronal cells and exert neuroprotective activity.<sup>15</sup> On the other hand, the analysis of cortical proteome changes afforded by HPPL in both TBI models clearly revealed its ability to downregulate many proteins/pathways linked to inflammation, synapses or mitochondria, which are initially upregulated post-injury, and confirmed, at a larger scale, our targeted gene expression analyses and biochemical studies. The common proteins downregulated by HPPL in both CCI and CBS

belong to a functional network related to fatty acid biosynthesis (Fig. 8D). These fatty acids are known for their ability to induce significant failures in various pathways related to energy metabolism.<sup>47</sup> Their levels are usually elevated following TBI.<sup>48,49</sup> Therefore, our finding suggests that HPPL might contribute to reduce lipotoxicity and, therefore, to limit energy failure and mitochondrial dysfunction. The diversity of the pathways associated with the neuroprotective activity of the platelet lysate was also illustrated by the ability of HPPL to modulate neuroinflammation processes by explicitly targeting the DAM and DAA (disease-associated microglia and astrocytes) signatures. Interestingly, we observed that 12 of the 23 DAM genes downregulated by HPPL in the CBS model belonged to a network associated to ribosome annotation (Supplementary Fig. 6B). This is in agreement with the observation that some of the 41 proteins upregulated in both TBI models and downregulated by HPPL in the two models belong to a network associated with translation (Fig. 8D). While the functional significance of this observation remains to be elucidated, recent works have highlighted that inappropriate microglial translation strongly perturbs neural networks and behaviour in mice.<sup>50</sup> All these positive effects of HPPL converged to functional improvements attested by behavioural tests. The latter revealed that HPPL treatment led to a significant improvement not only of motor functions, notably coordination, but also corrected memory impairment.

Functional improvements provided by the platelet proteome correlate with the physiological repair mechanisms of the injury microenvironment seen, for instance, in the use of a single trophic factor leading to behavioural recovery subsequent to a TBI.<sup>51</sup> Our data corroborate findings that an intracranial injection of a human platelet lysate stimulated neurogenesis and angiogenesis in a rat model of ischaemic stroke and could also enhance motor functions.<sup>52</sup> Such beneficial effects could reflect prosurvival and anti-apoptotic actions exerted on endogenous neural progenitor cells.<sup>53</sup> The human platelet proteome, which is rich in a range of neurotrophic factors, may also potentially promote neurogenesis by differentiation of the neurogenic niche, thereby stimulating neurogenesis in the dentate gyrus of the hippocampus.<sup>52</sup> The human platelet proteome in cellular models of amyotrophic lateral sclerosis and Parkinson's disease protected against apoptosis and ferroptosis cell death through Akt and mitogen-activated protein kinase (MEK) signalling,<sup>14,22,23</sup> enhanced expressions of tyrosine hydroxylase (TH) and neuron-specific enolase (NSE) in LUHMES cells,<sup>23</sup> was strongly neuroprotective of primary neurons exposed to elastin,<sup>23</sup> and decreased microglial inflammation after lipopolysaccharide stimulation and induction of neuronal cell differentiation.<sup>15</sup> The observation that HPPL administration resulted in biochemical and behavioural improvements in two distinct animal models suggests a broad therapeutic utility for both mild and intermediate TBIs. We propose that one treatment modality could include a single topical cranial administration, in cases of penetrating injury characterized by a breach of the skull and dura as in our CBS model, followed by intranasal administration. Alternatively, intracerebroventricular delivery (for prolonged therapy in severe cases) may be one alternative option to be evaluated in preclinical TBI models.

In conclusion, the HPPL exerted strong modulatory control of detrimental excessive inflammation and oxidative effects associated with a TBI, protected against neuronal damage, and improved motor neuron behaviour in two animal models. As such, the human platelet proteome may emerge as a pragmatic biotherapeutic approach to treat brain trauma, stroke, and other neurological disorders, as recently suggested.<sup>12,13,54</sup> Such clinical applications in neurology are supported by the fact that platelet concentrates for transfusion, which are used as raw materials for

preparing the platelet lysate, are an already licensed essential medicine for adults and children, with known quality and safety profiles<sup>55</sup> and available at a global level.

## Acknowledgements

We thank the Taipei Blood Center (Taiwan Blood Service Foundation, Guandu, Taiwan) for the supply of platelet concentrates. We also acknowledge the mass spectrometric technical research services from National Taiwan University (NTU) Consortia of Key Technologies and NTU Instrumentation Center. We thank Mr Man Hau Ho for the NADPH assay and Yen Hua Chen (Graduate Institute of Neural Regenerative Medicine, college of Medical Science and Technology, Taipei Medical University) for her technical support.

## Funding

Ministry of Science and Technology (MOST) of Taiwan (107-2314-B-038-084); Taipei Medical University (TMU) Higher Education Sprout Project MoE (DP2-107-21121-01N-09); PhD fellowship from TMU and Université de Lille, France (CABRI/MOBLILEX grant) to O.N.; Bilateral Orchid research project (MOST and French Association of Taiwan-Campus France; 108-2911-I-038-503); Inserm, Centre National de la Recherche Scientifique (CNRS), Université de Lille and Centre Hospitalier Universitaire (CHU) Lille (Programmes d'Investissements d'Avenir LabEx (excellence laboratory), DISTALZ (Development of Innovative Strategies for a Transdisciplinary approach to Alzheimer's disease)).

## Competing interests

M.L.C., D.D., and T.B. are named as inventors of patents applied by their respective academic institutions.

## Supplementary material

Supplementary material is available at *Brain* online.

## References

1. Michael CD, Abbas R, Saksham G, et al. Estimating the global incidence of traumatic brain injury. *J Neurosurgery*. 2019;130(4):1080–1097.
2. Rohling ML, Binder LM, Demakis GJ, Larrabee GJ, Ploetz DM, Langhinrichsen-Rohling J. A meta-analysis of neuropsychological outcome after mild traumatic brain injury: Re-analyses and reconsiderations of Binder et al. (1997), Frencham et al. (2005), and Pertab et al. (2009). *Clin Neuropsychol*. 2011;25(4):608–623.
3. Girgis F, Pace J, Sweet J, Miller JP. Hippocampal neurophysiologic changes after mild traumatic brain injury and potential neuromodulation treatment approaches. *Front Syst Neurosci*. 2016;10:8.
4. Sharma B, Changoor A, Monteiro L, Colella B, Green R. Prognostic-factors for neurodegeneration in chronic moderate-to-severe traumatic brain injury: A systematic review protocol. *Syst Rev*. 2020;9(1):23.
5. Faden AI, Loane DJ. Chronic neurodegeneration after traumatic brain injury: Alzheimer disease, chronic traumatic encephalopathy, or persistent neuroinflammation? *Neurotherapeutics*. 2015;12(1):143–150.

6. Carney N, Totten AM, O'Reilly C, et al. Guidelines for the management of severe traumatic brain injury, fourth edition. *Neurosurgery*. 2017;80(1):6–15.
7. Blennow K, Brody DL, Kochanek PM, et al. Traumatic brain injuries. *Nat Rev Dis Primers*. 2016;2:16084.
8. Nurden AT, Nurden P, Sanchez M, Andia I, Anitua E. Platelets and wound healing. *Front Biosci*. 2008;13:3532–3548.
9. Burnouf T, Goubran HA, Chen TM, Ou KL, El-Ekiaby M, Radosevic M. Blood-derived biomaterials and platelet growth factors in regenerative medicine. *Blood Rev*. 2013;27(2):77–89.
10. Burnouf T, Goubran HA, Chou ML, Devos D, Radosevic M. Platelet microparticles: Detection and assessment of their paradoxical functional roles in disease and regenerative medicine. *Blood Rev*. 2014;28(4):155–166.
11. Johnson J, Wu YW, Blyth C, Lichtfuss G, Goubran H, Burnouf T. Prospective therapeutic applications of platelet extracellular vesicles. *Trends Biotechnol*. 2021;39(6):598–612.
12. Leiter O, Walker TL. Platelets: The missing link between the blood and brain? *Prog Neurobiol*. 2019;183:101695.
13. Leiter O, Walker TL. Platelets in neurodegenerative conditions—friend or foe? *Front Immunol*. 2020;11:747.
14. Chou ML, Wu JW, Gouel F, et al. Tailor-made purified human platelet lysate concentrated in neurotrophins for treatment of Parkinson's disease. *Biomaterials*. 2017;142:77–89.
15. Nebie O, Barro L, Wu YW, et al. Heat-treated human platelet pellet lysate modulates microglia activation, favors wound healing and promotes neuronal differentiation in vitro. *Platelets*. 2020;32(2):226–212.
16. Song J, Li N, Xia Y, et al. Arctigenin confers neuroprotection against mechanical trauma injury in human neuroblastoma SH-SY5Y Cells by regulating miRNA-16 and miRNA-199a expression to alleviate inflammation. *J Mol Neurosci*. 2016;60(1):115–129.
17. KöRnyei Z, CziráK A, Vicsek T, Madarász E. Proliferative and migratory responses of astrocytes to in vitro injury. *J Neurosci Res*. 2000;61(4):421–429.
18. Deacon RMJ. Measuring motor coordination in mice. *J Vis Exp*. 2013;(75):e2609.
19. Liu X-F, Fawcett JR, Thorne RG, DeFor TA, Frey IIW. Intranasal administration of insulin-like growth factor-I bypasses the blood-brain barrier and protects against focal cerebral ischemic damage. *J Neurolog Sci*. 2001;187(1-2):91–97.
20. Lv Q, Fan X, Xu G, et al. Intranasal delivery of nerve growth factor attenuates aquaporins-4-induced edema following traumatic brain injury in rats. *Brain Res*. 2013;1493:80–89.
21. Hanson LR, Fine JM, Svitak AL, Faltesek KA. Intranasal administration of CNS therapeutics to awake mice. *J Vis Exp*. 2013;(74):4440.
22. Gouel F, Do Van B, Chou ML, et al. The protective effect of human platelet lysate in models of neurodegenerative disease: Involvement of the Akt and MEK pathways. *J Tissue Eng Regen Med*. 2017;11(11):3236–3240.
23. Nebie O, Devos D, Vingtdoux V, et al. The neuroprotective activity of heat-treated human platelet lysate biomaterials manufactured from outdated pathogen-reduced (amotosalen/UVA) platelet concentrates. *J Biomed Sci*. 2019;26(1):89.
24. Delila L, Wu YW, Nebie O, et al. Extensive characterization of the composition and functional activities of five preparations of human platelet lysates for dedicated clinical uses. *Platelets*. 2020;32(2):259–214.
25. Keren-Shaul H, Spinrad A, Weiner A, et al. A unique microglia type associated with restricting development of Alzheimer's disease. *Cell*. 2017;169(7):1276–1290.e17.
26. Habib N, McCabe C, Medina S, et al. Disease-associated astrocytes in Alzheimer's disease and aging. *Nature Neurosci*. 2020;23(6):701–706.
27. Sulhan S, Lyon KA, Shapiro LA, Huang JH. Neuroinflammation and blood-brain barrier disruption following traumatic brain injury: Pathophysiology and potential therapeutic targets. *J Neurosci Res*. 2020;98(1):19–28.
28. Dixon CE, Clifton GL, Lighthall JW, Yaghmai AA, Hayes RL. A controlled cortical impact model of traumatic brain injury in the rat. *J Neurosci Methods*. 1991;39(3):253–262.
29. Lim R, Miller JF, Zaheer A. Purification and characterization of glia maturation factor beta: A growth regulator for neurons and glia. *Proc Natl Acad Sci U S A*. 1989;86(10):3901–3905.
30. KuÅur M, Tanriverdi T, Dashti R, et al. Superoxide dismutase, catalase, and guanase in traumatic brain injury. *Neurosurg Q*. 2005;15:186–189.
31. Crespo-Diaz R, Behfar A, Butler GW, et al. Platelet lysate consisting of a natural repair proteome supports human mesenchymal stem cell proliferation and chromosomal stability. *Cell Transplant*. 2011;20(6):797–811.
32. Semple JW, Italiano JE Jr, Freedman J. Platelets and the immune continuum. *Nat Rev Immunol*. 2011;11(4):264–274.
33. García A, Prabhakar S, Brock CJ, et al. Extensive analysis of the human platelet proteome by two-dimensional gel electrophoresis and mass spectrometry. *Proteomics*. 2004;4(3):656–668.
34. Agrahari V, Agrahari V, Burnouf PA, Chew CH, Burnouf T. Extracellular microvesicles as new industrial therapeutic frontiers. *Trends Biotechnol*. 2019;37(7):707–729.
35. Agrahari V, Burnouf PA, Burnouf T, Agrahari V. Nanoformulation properties, characterization, and behavior in complex biological matrices: Challenges and opportunities for brain-targeted drug delivery applications and enhanced translational potential. *Adv Drug Deliv Rev*. 2019;148:146–180.
36. Vašiček O, Lojek A, Cíz M. Serotonin and its metabolites reduce oxidative stress in murine RAW264. 7 macrophages and prevent inflammation. *J Physiol Biochem*. 2020;76(1):49–60.
37. Smith JM, Lunga P, Story D, et al. Inosine promotes recovery of skilled motor function in a model of focal brain injury. *Brain*. 2007;130(Pt 4):915–925.
38. Kensler TW, Wakabayashi N, Biswal S. Cell survival responses to environmental stresses via the keap1-NRF2-ARE pathway. *Annu Rev Pharmacol Toxicol*. 2007;47(1):89–116.
39. Habtemariam S. Antioxidant and Anti-inflammatory mechanisms of neuroprotection by ursolic acid: Addressing brain injury, cerebral ischemia, cognition deficit, anxiety, and depression. *Oxid Med Cell Longev*. 2019;2019:8512048.
40. Saso L, Firuzi O. Pharmacological applications of antioxidants: Lights and shadows. *Curr Drug Targets*. 2014;15(13):1177–1199.
41. Moosavi F, Hosseini R, Saso L, Firuzi O. Modulation of neurotrophic signaling pathways by polyphenols. *Drug Des Devel Ther*. 2016;10:23–42.
42. Menet R, Lecordier S, ELAli A. Wnt pathway: An emerging player in vascular and traumatic mediated brain injuries. Review. *Front Physiol*. 2020;11(1149):565667.
43. Paganoni S, Bernstein J, Ferreira A. Ror1-Ror2 complexes modulate synapse formation in hippocampal neurons. *Neuroscience*. 2010;165(4):1261–1274.
44. Chang C-Y, Liang M-Z, Wu C-C, et al. WNT3A promotes neuronal regeneration upon traumatic brain injury. *Int J Mol Sci*. 2020;21(4):1463.
45. Zhang JY, Lee JH, Gu X, et al. Intranasally Delivered Wnt3a Improves Functional Recovery after Traumatic Brain Injury by Modulating Autophagic, Apoptotic, and Regenerative Pathways in the Mouse Brain. *J Neurotrauma*. 2018;35(5):802–813.
46. Zhao M-L, Chen S-J, Li X-H, et al. Optical depolarization of DCX-expressing cells promoted cognitive recovery and maturation

- of newborn neurons via the Wnt/ $\beta$ -catenin pathway. *J Alzheimer's Dis.* 2018;63(1):303–318.
47. Schuck PF, Ferreira GC, Moura AP, et al. Medium-chain fatty acids accumulating in MCAD deficiency elicit lipid and protein oxidative damage and decrease non-enzymatic antioxidant defenses in rat brain. *Neurochem Int.* 2009;54(8):519–525.
  48. González-Domínguez R. Medium-chain fatty acids as biomarkers of mitochondrial dysfunction in traumatic brain injury. *EBioMedicine.* 2016;12:8–9.
  49. Pilitsis JG, Coplin WM, O'Regan MH, et al. Free fatty acids in cerebrospinal fluids from patients with traumatic brain injury. *Neurosci Lett.* 2003;349(2):136–138.
  50. Xu Z-X, Kim GH, Tan J-W, et al. Elevated protein synthesis in microglia causes autism-like synaptic and behavioral aberrations. *Nat Commun.* 2020;11(1):1797.
  51. Cox CS Jr. Cellular therapy for traumatic neurological injury. *Pediatr Res.* 2018;83(1-2):325–332.
  52. Hayon Y, Dashevsky O, Shai E, Varon D, Leker RR. Platelet lysates stimulate angiogenesis, neurogenesis and neuroprotection after stroke. *Thromb Haemost.* 2013;110(2):323–330.
  53. Kazanis I, Feichtner M, Lange S, et al. Lesion-induced accumulation of platelets promotes survival of adult neural stem/progenitor cells. *Exp Neurol.* 2015;269:75–89.
  54. Gouel F, Rolland AS, Devedjian JC, Burnouf T, Devos D. Past and future of neurotrophic growth factors therapies in ALS: From single neurotrophic growth factor to stem cells and human platelet lysates. *Front Neurol.* 2019;10:835.
  55. WHO. WHO Model List of Essential Medicines. 2019. Accessed 30 September 2021. <https://www.who.int/groups/expert-committee-on-selection-and-use-of-essential-medicines/essential-medicines-lists>